

# Hydrodynamics of Dense Active Fluids: Turbulence-Like States and the Role of Advected Activity

Sandip Sahoo,<sup>1,\*</sup> Siddhartha Mukherjee,<sup>2,†</sup> and Samriddhi Sankar Ray<sup>1,‡</sup>

<sup>1</sup>*International Centre for Theoretical Sciences, Tata Institute of Fundamental Research, Bangalore 560089, India*

<sup>2</sup>*Department of Mechanical Engineering, Indian Institute of Technology Kanpur, Kanpur 208016, India*

Dense suspensions of self-propelled bacteria and related active fluids exhibit spontaneous flow generation, vortex formation, and spatiotemporally chaotic dynamics despite operating at vanishingly small Reynolds numbers. These phenomena, commonly referred to as active turbulence, display striking visual and statistical similarities to classical inertial turbulence while arising from fundamentally different nonequilibrium mechanisms. In this article, we present a combined review and theoretical study of hydrodynamic models for dense active fluids, with particular emphasis on bacterial suspensions described by the Toner–Tu–Swift–Hohenberg (TTSH) framework. We review key experimental and theoretical developments underlying the analogy between active and inertial turbulence, highlighting the emergence of multiple dynamical regimes and the conditions under which universal spectral and intermittent behavior arises in homogeneous systems. Moving beyond the conventional assumption of spatially uniform activity, we introduce a minimal model in which the activity field is heterogeneous and dynamically advected by the flow it generates. Thus treating activity as a spatiotemporally evolving field coupled to the TTSH dynamics, we investigate how advection and diffusion lead to sharp activity fronts, confinement of turbulent motion, and complex interfacial morphologies. Our numerical results demonstrate that spatial variations in activity can induce transient coexistence of distinct spectral regimes and that universality in active turbulence is inherently local and time-dependent in heterogeneous systems. These findings underscore the importance of treating activity as a dynamical field in its own right and provide a framework for studying active turbulence in more realistic, spatially structured biological and synthetic active matter systems.

## I. INTRODUCTION

Active matter systems consist of agents that convert stored or ambient energy into systematic motion at the microscopic scale [1–6]. Prominent examples include bacterial suspensions [7], cytoskeletal extracts driven by molecular motors [8], synthetic Janus particles [9], and vibrated granular media [10]. Unlike equilibrium systems, active matter is intrinsically out of equilibrium: Detailed balance is broken locally, and energy injection occurs continuously at the level of individual constituents. As a result, active systems exhibit collective phenomena — such as flocking [11–13], swarming [14–16], phase separation [17–19], and spontaneous flow generation [20–23] — that have no direct equilibrium analogues.

Among these systems, dense suspensions of swimming bacteria occupy a special place. When bacterial concentration is sufficiently high, individual swimming trajectories become strongly coupled through steric interactions, near-field hydrodynamics, and self-generated flow fields [4, 6]. Experiments on quasi-two-dimensional bacterial films have repeatedly shown the emergence of vortices, jets, and spatiotemporally chaotic patterns at length scales much larger than the size of a single swimmer. Remarkably, these flows arise in a regime where the Reynolds number, based on both swimmer size and col-

lective velocity scales, remains exceedingly small. This apparent contradiction — turbulence-like motion in the absence of inertia and at negligible Reynolds numbers — has motivated extensive experimental, numerical, and theoretical investigation over the past decade [6, 7, 16, 24–31].

Early theoretical descriptions of collective motion in active systems focused on flocking and long-range orientational order, most notably within the Toner–Tu framework [32, 33]. These theories successfully capture the onset of collective motion and the emergence of polar order in dry active systems, where momentum is not conserved. However, dense bacterial suspensions typically do not settle into uniformly ordered states. Instead, they exhibit sustained chaotic dynamics characterized by the continuous creation and annihilation of vortices, a well-defined mesoscale length, and broadband velocity fluctuations. Capturing these features requires continuum descriptions that go beyond homogeneous flocking and explicitly incorporate pattern-forming instabilities [4, 6].

A significant advance in this direction was the realization that active stresses generated by extensile swimmers can effectively act as negative viscosity, destabilizing long-wavelength modes of the flow. When supplemented by higher-order stabilizing gradients, this leads naturally to a hydrodynamic description closely related to the Swift–Hohenberg equation [34, 35], but augmented by the nonlinear advection and symmetry-breaking terms characteristic of active matter. The resulting Toner–Tu–Swift–Hohenberg (TTSH) framework [24, 25], which we review in the next section, has emerged as a minimal con-

---

\* sandipsahoo09902@gmail.com

† smukherjee@iitk.ac.in

‡ samriddhisankarray@gmail.com

tinuum model capable of reproducing many qualitative and quantitative features of dense bacterial turbulence, including vortex formation [26–31].

Parallel to these theoretical developments, an analogy between active turbulence and classical inertial turbulence gradually emerged. Early experimental and numerical studies focused primarily on energy spectra in dense bacterial flows and reported apparent power-law scaling over intermediate ranges [24–26]. However, the corresponding scaling exponents were found to depend sensitively on the level of activity, and the flows were largely non-intermittent, indicating only a partial and qualitative resemblance to high Reynolds number turbulence.

Subsequent investigations [28–31] refined this picture by revealing a more nuanced scenario. In particular, it was shown that beyond a critical level of activity, active turbulent flows undergo a qualitative transition: The scaling exponents of the energy spectra become universal [30] and essentially independent of activity, while strong intermittency develops in both Eulerian and Lagrangian statistics [30, 31]. In this high-activity regime, active turbulence exhibits statistical features that more closely parallel those of inertial turbulence, despite the absence of inertia and the fundamentally different mechanisms of energy injection and dissipation. Active turbulence thus spans multiple dynamical regimes and constitutes a distinct, yet deeply connected, class of chaotic flow phenomena [6].

Most existing theoretical and numerical studies of active turbulence, however, rely on a crucial simplifying assumption: The activity is taken to be spatially uniform and temporally constant [6]. This assumption is reasonable for well-mixed bacterial suspensions under controlled laboratory conditions, but it is rarely satisfied in natural or biologically relevant settings [36]. In real bacterial colonies, activity can vary due to nutrient gradients, oxygen availability, or local crowding [37–43]. Similarly, in synthetic active systems, spatial modulation of activity can be externally imposed through light, chemical cues, or patterned substrates [44–52]. These considerations raise fundamental questions: How does spatially heterogeneous activity modify the structure and statistics of active turbulence? Can activity itself behave as a dynamically evolving field, transported by the flow it generates? And, to what extent can such an activity field be viewed as an active or passive scalar in a turbulent-like environment?

In this work, we combine a semi-review of active turbulence with new theoretical and numerical results on heterogeneously active suspensions. We first recall the pedagogy of the TTSH hydrodynamic framework for dense bacterial suspensions and review key developments underpinning the analogy between active and inertial turbulence. We then move beyond the constant-activity paradigm and introduce models in which the activity field is spatially varying and dynamically advected by the flow. We investigate how such advected activity fields evolve,

homogenize, or form sharp fronts, and we characterize the resulting flow structures and scaling properties.

The paper is organized as follows. In Sec.(II), we derive the Toner–Tu–Swift–Hohenberg hydrodynamic equations appropriate for dense bacterial suspensions. Section (III) reviews the development of the turbulence analogy in active matter, focusing on key experimental and theoretical milestones. In Sec.(IV), we discuss the limitations of uniform-activity models and motivate the need for heterogeneous descriptions. Section (V) introduces a minimal advection model for spatially varying activity. Our main results are presented in Sec.(VI), where we analyze the evolution, mixing, and front dynamics of the activity field and their impact on active turbulence. Finally, Sec.(VII) summarizes our findings and outlines open questions and future directions.

## II. HYDRODYNAMIC THEORY FOR DENSE BACTERIAL SUSPENSIONS: A SHORT REVIEW

Dense suspensions of swimming bacteria exhibit collective dynamics that differ qualitatively from both dilute active gases and equilibrium fluids. At sufficiently high volume fractions, steric interactions, near-field hydrodynamics, and self-generated flows lead to the emergence of mesoscale vortices, jets, and spatiotemporally chaotic patterns commonly referred to as *bacterial turbulence*. Despite the low Reynolds number of the individual swimmers, these systems display features reminiscent of inertial turbulence, albeit governed by entirely different physical mechanisms.

A successful continuum description of such systems must therefore (i) incorporate spontaneous polar ordering due to self-propulsion, (ii) account for momentum injection at the swimmer scale, and (iii) include nonlinear saturation and pattern-selection mechanisms. These requirements are naturally met by a hybrid hydrodynamic framework combining elements of the Toner–Tu theory of flocking with Swift–Hohenberg-type gradient terms. In this section, we briefly review this Toner–Tu–Swift–Hohenberg (TTSH) model starting from symmetry arguments and coarse-grained conservation laws [24, 25]; we refer the reader to the review article by Alert, Casademunt, and Joanny [6] for a detailed modern review of this field.

We consider a dense suspension of self-propelled bacteria confined to a thin film or quasi-two-dimensional geometry, as is common in experiments. The relevant coarse-grained fields are:

- the bacterial number density  $\rho(\mathbf{r}, t)$ ,
- the polarization (or mean velocity) field  $\mathbf{v}(\mathbf{r}, t)$ .

At high densities, density fluctuations are strongly suppressed due to steric constraints, allowing one to work in the incompressible or weakly compressible limit. We therefore assume  $\rho \simeq \rho_0$  constant and focus on the

dynamics of  $\mathbf{v}$ , which simultaneously represents the local orientational order and the coarse-grained flow field. Number conservation implies

$$\partial_t \rho + \nabla \cdot (\rho \mathbf{v}) = 0, \quad (1)$$

which reduces to  $\nabla \cdot \mathbf{v} = 0$  in the incompressible limit.

In the absence of momentum conservation (neglecting friction with the substrate or a surrounding fluid), the velocity field obeys relaxational rather than Navier–Stokes dynamics. The most general equation of motion for  $\mathbf{v}$ , consistent with rotational invariance and broken Galilean invariance, is given by the Toner–Tu equation:

$$\begin{aligned} \partial_t \mathbf{v} + \lambda_1 (\mathbf{v} \cdot \nabla) \mathbf{v} + \lambda_2 (\nabla \cdot \mathbf{v}) \mathbf{v} + \lambda_3 \nabla |\mathbf{v}|^2 \\ = -\nabla p - (\alpha + \beta |\mathbf{v}|^2) \mathbf{v} + D \nabla^2 \mathbf{v}. \end{aligned} \quad (2)$$

Here,  $\alpha < 0$  controls the linear instability toward collective motion, while  $\beta > 0$  saturates the growth of  $\mathbf{v}$ . The coefficients  $\lambda_i$  encode the absence of Galilean invariance typical of active matter systems [24]. The pressure  $p$  enforces incompressibility. For  $\alpha < 0$ , Eq. (2) admits a homogeneous polar state  $|\mathbf{v}| = \sqrt{|\alpha|/\beta}$ , corresponding to coherent flocking. However, dense bacterial suspensions rarely settle into such uniform states. Instead, they exhibit vortex patterns with a well-defined characteristic length scale, which the Toner–Tu theory alone cannot capture.

Experimental studies indicate that active stresses generated by extensile swimmers effectively reduce the viscosity of the suspension. At high activity, this can lead to a *negative effective viscosity*, destabilizing long-wavelength modes. To account for this, the diffusion term is generalized as  $\Gamma_0 \nabla^2 \mathbf{v}$ , with  $\Gamma_0 < 0$ . A linear stability analysis of Eq. (2) around  $\mathbf{v} = 0$  then yields a growth rate

$$\sigma(k) = -(\alpha + \Gamma_0 k^2), \quad (3)$$

which is *positive* for all wavelengths as long as  $\alpha < 0$  and  $\Gamma_0 < 0$ . This implies unbounded growth of modes, and hence ill-posed dynamics unless higher-order stabilizing terms are included.

To regularize the instability and select a finite vortex scale, we introduce the leading higher-order gradient term  $\Gamma_2 \nabla^4 \mathbf{v}$  allowed by symmetry with  $\Gamma_2 > 0$ . The resulting linear dispersion relation becomes

$$\sigma(k) = -(\alpha + \Gamma_0 k^2 + \Gamma_2 k^4), \quad (4)$$

which is maximized at a finite wavenumber

$$k_c = \sqrt{\frac{|\Gamma_0|}{2\Gamma_2}}. \quad (5)$$

This is the hallmark of Swift–Hohenberg dynamics and leads to spontaneous pattern formation with a characteristic length scale  $\ell_c \sim k_c^{-1}$ , consistent with experimental observations of bacterial vortices.

Collecting all terms, the full TTSH equation for dense bacterial suspensions reads

$$\partial_t \mathbf{v} + \lambda_1 (\mathbf{v} \cdot \nabla) \mathbf{v} = -\nabla p - (\alpha + \beta |\mathbf{v}|^2) \mathbf{v} + \Gamma_0 \nabla^2 \mathbf{v} - \Gamma_2 \nabla^4 \mathbf{v}, \quad (6)$$

supplemented by the incompressibility constraint  $\nabla \cdot \mathbf{v} = 0$ .

Equation (6) constitutes a minimal continuum model for mesoscale bacterial turbulence. The nonlinear advection term transfers energy across scales, while the competition between  $\Gamma_0 < 0$  and  $\Gamma_2 > 0$  injects energy at a finite wavelength. The cubic nonlinearity saturates the instability and prevents blow-up.

The TTSH framework provides a unified description of dense active fluids that bridges polar flocking and pattern-forming instabilities. It is valid on length-scales that are large compared to the swimmer sizes and timescales longer than their reorientation time. While derived phenomenologically, several coefficients can be related to microscopic parameters such as swim speed, dipolar force strength, and rotational diffusivity.

Importantly, the model leads to an inverse energy flux in two dimensions and reproduces key statistical features of bacterial turbulence, including non-Gaussian velocity distributions and scale-dependent energy spectra. As such, it has emerged as a canonical hydrodynamic description for dense bacterial suspensions and related active fluids.

### III. ANALOGY BETWEEN ACTIVE AND INERTIAL TURBULENCE: KEY DEVELOPMENTS

A central theme in active fluid research is the analogy between spatiotemporally chaotic flows in dense suspensions and classical, high Reynolds number turbulence. Although the underlying physical mechanisms differ — active flows are driven by internal energy injection at the microscale, whereas inertial turbulence emerges from nonlinear momentum transfer from large to small scales at high Reynolds numbers — several statistical and structural similarities have motivated comparative studies. Below we review a few key contributions that cement and critically evaluate this analogy.

In a landmark study [24], Wensink and collaborators combined experiments on dense *Bacillus subtilis* suspensions with particle simulations and continuum theory to characterize what they termed “mesoscale turbulence in living fluids”. They measured energy spectra and velocity structure functions in quasi-two-dimensional geometries and found broad-band kinetic energy across intermediate wavenumbers, reminiscent of inertial turbulence spectra. Their experiments revealed vortical structures with a characteristic mesoscopic scale and nontrivial correlations in the flow field, suggesting that chaotic bacterial dynamics could share statistical signatures with conventional turbulence despite the absence of inertia. Based on these observations, they proposed a minimal

continuum model for incompressible active bacterial flow and demonstrated that it reproduces many experimentally observed statistical features of active turbulence.

This study laid the groundwork for viewing bacterial turbulence not simply as random motion but as a distinct nonequilibrium phase with well-defined statistical properties. Importantly, it catalyzed subsequent theoretical efforts to generalize active hydrodynamics beyond simple Toner-Tu models to incorporate turbulence-like spatiotemporal chaos [27–31, 53–57].

Bratanov *et al.* [26] formulated a more systematic comparison between active turbulent flows and inertial turbulence by extending continuum descriptions to include both the usual Navier-Stokes nonlinearity and active stress contributions allowed by symmetry. They demonstrated that the interaction between the quadratic convective term from Navier-Stokes and the cubic nonlinearity stemming from active stresses leads to energy spectra at large scales exhibiting power-law regimes, albeit with nonuniversal exponents dependent on system parameters and finite-size effects.

This result highlighted that although active turbulence shares some spectral features with inertial turbulence, such as cascades or broad power-law-like ranges, the scaling laws and universality classes can differ fundamentally. In particular, active turbulence defines a distinct class of turbulent flows where energy injection occurs at the microscale via self-propulsion, and the scaling exponents are set by non-equilibrium organization rather than inertial transfer alone.

Building on these insights, Mukherjee *et al.* [30] and Kiran *et al.* [31] investigated the emergence of a universal chaotic regime in active turbulence when activity exceeds a critical level. Their studies suggest that, beyond a threshold of activity, active flows transition into highly intermittent states with non-Gaussian velocity distributions [31] and chaotic fluctuations that mimic classical turbulence intermittency — albeit driven by internal energy injection rather than inertial mechanisms. Such work indicates that active turbulence may exhibit its own version of intermittency universality, not tied directly to classical Kolmogorov scaling and phenomenology, but rather emergent from the interplay between active drive, nonlinear advection, and dissipation.

Using such hydrodynamic models, several studies have also shown that Lagrangian statistics [28, 29, 31, 58] in active turbulence bear unique signatures of the underlying nonequilibrium dynamics. For example, analysis of Lagrangian tracer trajectories reveals super-diffusive scaling and Lévy walk-like behavior over intermediate time scales, in stark contrast to the near-diffusive behavior typical of high Reynolds number flows [28, 29]. This super-diffusion can obscure the crossover from ballistic to diffusive motion and is tied to transient coherent structures in the flow that actively mold the tracer dynamics. Such features underscore key distinctions between active and inertial turbulent transport, even when Eulerian velocity fields exhibit similar-looking chaotic patterns.

Collectively, such studies illustrate both the power and the limits of the analogy between active and inertial turbulence. On the one hand, dense bacterial suspensions can exhibit spectra, mesoscale vortical organization, chaotic transport and universal turbulence statistics at sufficiently high activity, reminiscent of high Reynolds number flows. On the other hand, key features such as nonuniversal scaling, Lévy-type Lagrangian statistics, and activity-induced intermittency highlight fundamental differences rooted in the mechanisms of energy injection and dissipation. The active turbulence paradigm hence stands as a distinct universality class of chaotic fluid motion, connected to but not subsumed by classical turbulence theory.

#### IV. BEYOND A CONSTANT-ACTIVITY PARADIGM: HETEROGENEOUS SUSPENSIONS

Most theoretical and numerical studies of active turbulence assume that the activity parameter is spatially uniform and constant in time. This simplifying assumption has played a crucial role in establishing minimal hydrodynamic descriptions and identifying key dynamical regimes, as illustrated in the previous section. However, this paradigm represents an idealization that is rarely realized in experimental or biological settings.

In practice, activity in active matter systems is almost always heterogeneous [37–43]. In bacterial suspensions, local activity depends on nutrient availability, oxygen concentration, waste accumulation, and local crowding, all of which can vary significantly in space and time. Similarly, in synthetic active systems, activity can be externally modulated using light, chemical gradients, or patterned substrates, leading to controlled but intrinsically heterogeneous activity landscapes. Even in nominally uniform experimental preparations, finite-size effects and boundary interactions inevitably generate spatial variations in activity.

Despite its experimental relevance, the impact of spatially varying activity on active turbulence has only recently begun to be explored in a systematic manner. A notable step in this direction is the recent work of Mukherjee *et al.* [36], which explicitly relaxes the assumption of homogeneous activity and investigates dense active flows subject to spatially heterogeneous driving. Motivated by experimental situations in which activity is localized or externally patterned [40, 47, 59–61], this study demonstrates that activity heterogeneity fundamentally alters the structure of active turbulent states. In particular, regions of high activity act as localized sources of chaotic motion, while surrounding weakly active regions remain comparatively quiescent, leading to the emergence of sharp dynamical interfaces separating distinct flow regimes.

An important insight from this work is that these interfaces are not static boundaries but fluctuate strongly in time,

The most important insight from this work is that these interfaces exhibit rich dynamics, exhibiting intermittency and a complex spatio-temporal structure. As a result, heterogeneous activity introduces new physical ingredients into active turbulence, including confinement of vorticity, interface-dominated transport, and nontrivial mixing between active and inactive regions. Such effects have no direct analogue in homogeneous models and cannot be captured by treating activity as a single global control parameter.

At the same time, the activity heterogeneity considered in Ref. [36] is quenched in space, representing systems in which activity variations are imposed externally and remain fixed in time. While this is a natural and experimentally relevant starting point, particularly with the aim of active matter control, many active systems operate in a different regime, where activity itself can be transported, deformed, and mixed by the flow it generates. In bacterial suspensions, for instance, local activity can spread through advection of bacteria, while diffusion and growth processes concurrently act to smoothen or sharpen activity gradients.

This observation motivates a complementary perspective in which activity is treated as a dynamical field rather than a prescribed spatial pattern. In such a setting, the flow not only responds to activity gradients but also actively reshapes them, leading to a two-way coupling between turbulence and activity distribution. Understanding how this coupling modifies flow organization, intermittency, and spectral properties requires going beyond both homogeneous-activity models and quenched-heterogeneity approaches.

In the following sections, we adopt this viewpoint and study active turbulence in the presence of an advected, spatially varying activity field. This framework allows us to bridge homogeneous active turbulence and systems with fixed activity heterogeneity, and to address how transient fronts, mixing, and homogenization of activity influence the emergence, persistence, and eventual loss of turbulent behavior.

## V. AN ADVECTION MODEL FOR HETEROGENEOUSLY ACTIVE TURBULENCE

We introduce a minimal continuum framework in which the activity field is treated as a spatiotemporally evolving scalar coupled to the Toner–Tu–Swift–Hohenberg dynamics, which makes activity not merely a static control parameter but a dynamical quantity that can be transported, deformed, and mixed by the flow it generates. We consider the activity parameter  $\alpha$  appearing in Eq. (6) to be a coarse-grained field  $\alpha(\mathbf{x}, t)$ , representing the local strength of active driving. Physically, this field may encode variations in swimmer concentration, metabolic activity, nutrient availability, or externally imposed control parameters such as light intensity in synthetic active systems. In contrast to homogeneous

models, where  $\alpha$  is taken to be constant, here  $\alpha(\mathbf{x}, t)$  is allowed to vary continuously in space and time. In the absence of flow, spatial variations in activity would relax through diffusive processes associated with microscopic motion, growth, or chemical transport. In the presence of a chaotic velocity field, however, activity gradients can be strongly distorted and advected, leading to complex spatiotemporal structures analogous to those encountered in scalar mixing problems.

To capture these effects in the simplest possible manner, we model the evolution of the activity field using an advection–diffusion equation,

$$\partial_t \alpha + \mathbf{v} \cdot \nabla \alpha = \kappa \nabla^2 \alpha, \quad (7)$$

where  $\mathbf{v}(\mathbf{x}, t)$  is the velocity field governed by Eq. (6), and  $\kappa$  is an effective diffusivity associated with activity transport. Equation (7) represents a minimal description in which activity is transported by the flow while undergoing diffusive smoothing at small scales. No explicit source or sink terms are included, allowing us to isolate the role of advection and diffusion in shaping activity heterogeneity and to focus on how turbulent-like flows redistribute activity.

The relative importance of advective stretching and diffusive regularization is conveniently characterized by Schmidt number,  $Sc = \frac{|\Gamma_0|}{\kappa}$ , where  $\Gamma_0$  denotes a characteristic viscosity scale of the velocity field. Large Schmidt numbers correspond to weak diffusion, in which activity gradients can persist and sharpen under the action of the flow, while small Schmidt numbers lead to smoother and more rapidly homogenized activity fields.

The coupling between the activity field and the velocity dynamics arises entirely through the dependence of Eq. (6) on the local value of  $\alpha(\mathbf{x}, t)$ . Spatial variations in activity therefore modulate the linear instability and energy injection into the flow, leading to regions of the domain that support qualitatively different dynamical regimes. In turn, the resulting velocity field advects, stretches, and mixes the activity field through Eq. (7). This two-way coupling establishes a nontrivial feedback loop: Activity heterogeneity organizes the flow by localizing or suppressing turbulent motion, while the flow continuously reshapes the activity distribution.

In this sense, the activity field behaves as an *active scalar*. Although its evolution equation resembles that of a passively advected field, its spatial distribution directly controls where and how turbulent dynamics are generated. This minimal framework allows us to systematically investigate how the interplay between advection, diffusion, and activity-dependent forcing gives rise to evolving activity fronts, flow confinement, and modifications of spectral and statistical properties.

We perform direct numerical simulations (DNSs) of the coupled equations (6) and (7) on square periodic domains of length  $L = 20$  and  $30$ , discretized over  $N^2 = 1024^2$  and  $2048^2$  collocation points, respectively. Although the results presented here are drawn from the larger simu-

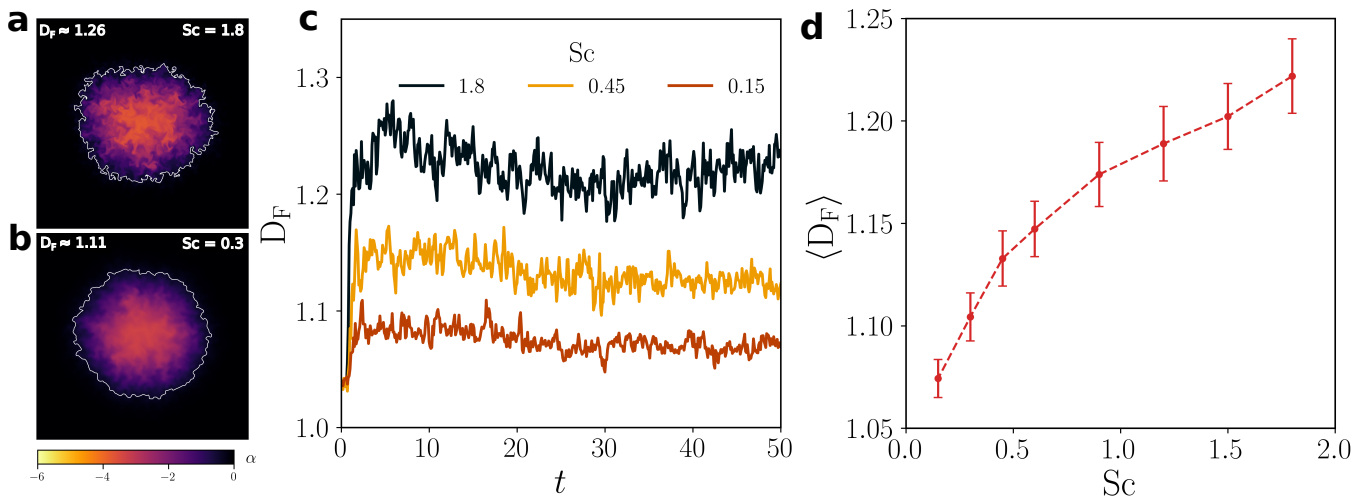


FIG. 1. Representative plots of the activity field  $\alpha$  at time  $t = 15$  for Schmidt numbers (a)  $Sc = 1.8$  and (b)  $Sc = 0.3$ , with the white curve denoting an iso-contour of the activity field defining the evolving activity front. The Schmidt number controls the morphology of this front, which becomes increasingly convoluted as diffusion weakens. This is best seen in a time evolution of the scalar field for a large range of Schmidt numbers as shown in Ref. [62]. Panel (c) shows the temporal evolution of the fractal dimension  $D_F$  of the activity front for different Schmidt numbers, illustrating a rapid growth from the initially smooth interface followed by saturation to a statistically steady value. Panel (d) shows the corresponding steady-state values of  $\langle D_F \rangle$ , with error bars characterizing statistical fluctuations, as a function of the Schmidt number. The activity fronts become more fractal with increasing  $Sc$ .

lation, they are consistent across both system sizes. A standard 1/2-de-aliased pseudo-spectral algorithm is applied to (6) to account for the cubic non-linearity in the coarse-grained velocity field, while a 2/3-de-aliased pseudo-spectral algorithm handles the quadratic non-linearity arising from the activity advection by the velocity field in (7). The time integration is carried out using a second-order Integrating Factor Runge-Kutta (IFRK2) scheme with a time step  $\delta t = 0.0002$ . The simulation parameters are kept identical to those used in the previous studies:  $\Gamma_0 = -0.045$ ,  $\Gamma_2 = |\Gamma_0|^3$ ,  $\beta = 0.5$  and  $\lambda_1 = 3.5$ . The heterogeneous activity field is initialized with  $\alpha_{\text{in}} = -6$  within a central disc of radius  $r = 5$  and  $\alpha_{\text{out}} = 0$  in the outside region. This configuration is particularly useful for analyzing the front morphologies and flow organization. A second initialization — with  $\alpha_{\text{in}} = -8$  inside a disc of radius  $r = 10$  and  $\alpha_{\text{out}} = 4$  outside — is employed to investigate the spectral features of the flow while preserving the underlying physics.

## VI. RESULTS

We now present results from numerical simulations of the Toner–Tu–Swift–Hohenberg equation (6), coupled to a dynamically evolving activity field (7). In contrast to the conventional homogeneous-activity formulation, the activity  $\alpha(\mathbf{x}, t)$  here obeys an advection–diffusion equation with diffusivity  $\kappa$  and is transported by the velocity field generated through Eq. (6). The resulting dynamics are governed by a nontrivial feedback loop: Spatial vari-

ations in activity modify the flow field, while the flow in turn advects, stretches, and deforms the activity distribution. This interplay leads to the formation of sharp activity fronts, heterogeneous flow structures, and complex interfacial morphologies, as illustrated in Figs. 1 and 2.

### A. Growth and morphological evolution of activity fronts

We begin with a qualitative characterization of the activity field and its associated fronts, focusing on the role of advection and diffusion in shaping their evolution. The system is initialized with activity concentrated within a circular region at the center of the domain, surrounded by a background of lower activity. This configuration defines a well-posed initial interface separating regions of high and low activity, allowing us to track the subsequent growth and deformation of the activity front.

Representative snapshots of the activity field  $\alpha(\mathbf{x}, t)$  at a fixed time are shown in Fig. 1(a) and (b) for two different Schmidt numbers. For a complete visualisation of how such fields evolve for a wide range of Schmidt numbers, we refer the reader to the animation found in Ref. [62]. At early times, the initially smooth circular interface is rapidly distorted by the flow generated within the active region. The activity patch is stretched, folded, and advected outward, in close analogy with scalar mixing in turbulent flows. We recall that similar interfaces are seen in high Reynolds number flows such as the boundaries between jets in  $\beta$ -plane

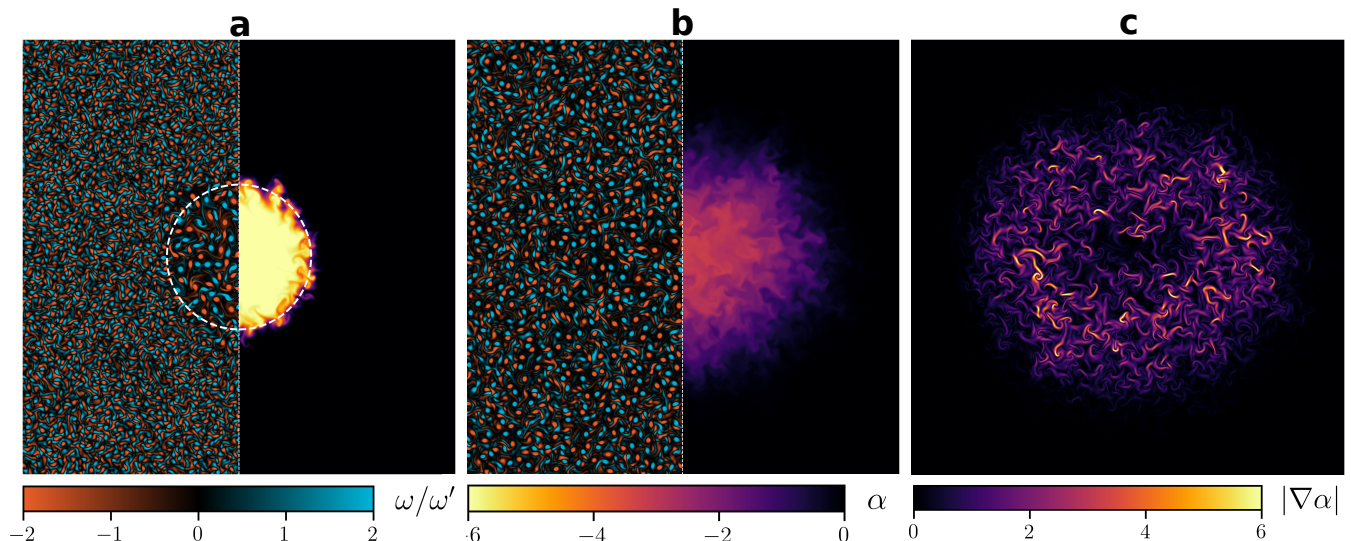


FIG. 2. Representative plots of the (normalized) vorticity field (left panels) and activity field (right panels) for Schmidt number  $Sc = 1.8$  at (a)  $t = 1.0$  and (b)  $t = 20.0$ . At early times, the turbulent flow is largely confined within the region of high activity, indicated by the white broken line in panel (a), while the surrounding region remains comparatively quiescent. At later times, as the activity spreads and becomes more homogeneous, this confinement weakens and vorticity structures extend more uniformly across the domain. Panel (c) shows the magnitude of the activity gradient field,  $|\nabla\alpha|$ , at  $t = 20$ , revealing intermittent, worm-like structures associated with sharp activity fronts. We refer the reader to Ref. [63] for a complete time evolution of the vorticity, activity and gradient of activity fields.

zonal turbulence [64] and turbulent/non-turbulent interfaces in mixing layers [65–69]. As a result, the interface separating high and low-activity regions evolves into a highly convoluted front, characterized by elongated filaments and sharp gradients.

The degree of interfacial roughening is strongly controlled by the Schmidt number. For lower  $Sc$ , diffusion acts efficiently to smoothen gradients, leading to comparatively regular and rounded fronts. As  $Sc$  is increased and diffusion weakens, advective stretching dominates, producing increasingly intricate front geometries with fine-scale structures. These fronts develop narrow filaments and deep indentations, indicative of repeated stretching and folding by the underlying chaotic flow.

The growth of sharp activity gradients is evident from the activity front defined as the iso-contour  $\alpha = -0.4$ , shown as white curves in Fig. 1(a) and (b). These fronts behave as dynamically evolving interfaces whose geometry reflects the competition between advective deformation and diffusive smoothing. Importantly, because activity directly feeds back onto the velocity field, the front is not merely passively transported: Regions of strong gradients and high curvature actively influence the local flow, further enhancing interfacial complexity.

To quantify this morphological evolution, we analyze the geometry of the activity front using a box-counting approach to extract its fractal dimension. The temporal evolution of the fractal dimension  $D_F$  is shown in Fig. 1(c) for different Schmidt numbers. Starting from an initially smooth interface,  $D_F$  grows rapidly as the front becomes increasingly wrinkled and irregular. After

a transient growth phase, the fractal dimension saturates to a statistically steady value, indicating the emergence of distinct a self-similar interfacial morphology during the mixing process.

Figure 1(d) summarizes the dependence of the steady-state fractal dimension on the Schmidt number. As expected, the fronts become more fractal as  $Sc$  increases: Reduced diffusion allows the flow to sustain finer interfacial structures before they are smoothed out. The systematic increase of  $D_F$  with  $Sc$  demonstrates that the geometry of activity fronts is a robust outcome of the coupled advection–activity dynamics.

## B. Flow organization and confinement by heterogeneous activity

While Fig. 1 emphasizes the evolution of activity fronts and their interfacial morphology, Fig. 2 illustrates how the velocity and vorticity fields respond to, and co-evolve with, the spreading activity. Together, these figures highlight the two-way coupling between activity heterogeneity and flow organization that distinguishes this system from homogeneous active turbulence.

Figures 2(a) and (b) shows representative snapshots of the normalized vorticity field (left panels) alongside the activity field (right panels) for a fixed Schmidt number,  $Sc = 1.8$ , at two different times. At early times (Fig. 2(a)), the activity remains strongly localized within a ring-like region surrounding the initial active patch. Correspondingly, the vorticity field is largely confined to

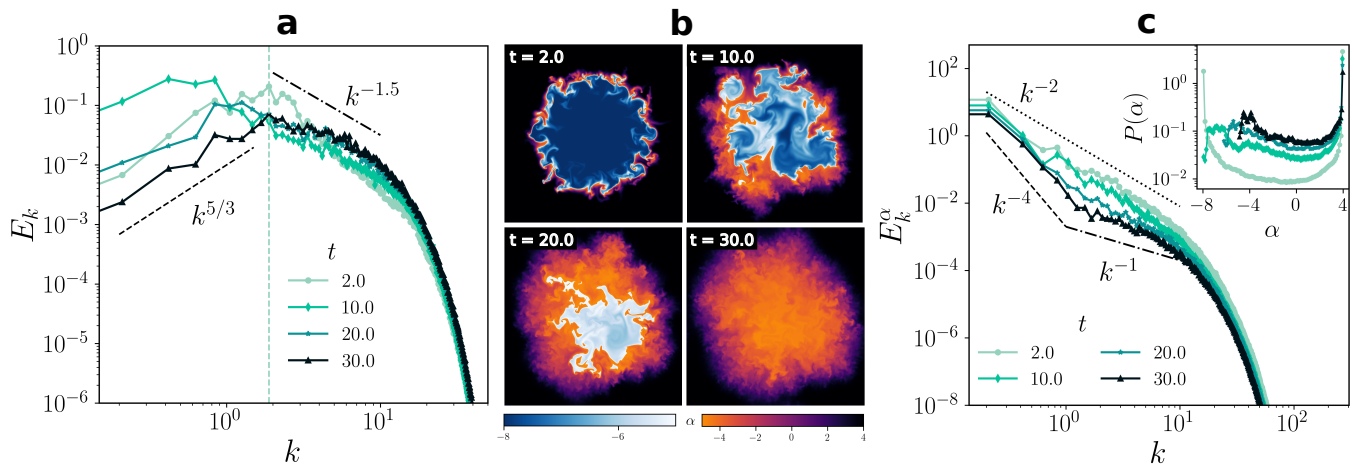


FIG. 3. (a) Kinetic energy spectra  $E(k)$  at four representative times for a system initialized with a strongly active patch of activity  $\alpha_{\text{in}} = -8$  inside a central disc of radius  $r = 10$  and  $\alpha_{\text{out}} = 4$  outside. This extreme value is chosen to clearly expose the mechanism underlying dual scaling. At early times, the spectrum exhibits two distinct regimes: a universal  $k^{-3/2}$  scaling at larger wavenumbers, characteristic of strongly active turbulence ( $\alpha < \alpha_c \approx -5$ ), and a non-universal scaling at smaller wavenumbers associated with weakly active regions. The crossover between these regimes occurs at a time-dependent wavenumber  $k_R(t) \sim R^{-1}(t)$ , where  $R(t)$  is the effective linear size of the region with  $\alpha < \alpha_c$ . As shown in panel (b),  $R(t)$  initially grows due to advection, causing  $k_R(t)$  to shift to smaller values, and later decreases as diffusion and mixing erode the strongly active core, shifting  $k_R(t)$  back to larger values and eventually eliminating the  $k^{-3/2}$  regime. (b) Snapshots of the activity field  $\alpha(\mathbf{x}, t)$  at the same four times, with regions satisfying  $\alpha < \alpha_c$  highlighted in blue. These blue regions define  $R(t)$  and thus directly set the crossover scale  $k_R(t)$  observed in panel (a): their growth supports the coexistence of dual spectral scaling, while their eventual shrinkage explains the disappearance of the universal regime. (c) The  $\alpha$ -spectrum shown at times as in panels (a) and (b) show distinct scaling regimes  $k^{-2}$  (dotted line),  $k^{-4}$  (dashed line) and  $k^{-1}$  (dot-dashed line). (Inset) Probability density functions (PDFs) of  $\alpha$  at these times, showing an initially near-bimodal distribution reflecting the coexistence of strongly and weakly active regions, which progressively flattens and eventually disappears for  $\alpha \lesssim \alpha_c$ , as the activity field becomes well mixed.

this high-activity domain, while the flow outside remains comparatively quiescent. This reflects the role of activity as a local source of instability and energy injection in the TTSH dynamics.

Within the active region, the vorticity field exhibits characteristic features of highly active turbulence, including coherent vortices and elongated streak-like structures. In contrast, regions of lower activity support weaker, less organized vorticity with distinctly different morphology. The sharp transition between these two dynamical regimes closely follows the activity front, emphasizing that the activity field effectively partitions the domain into dynamically distinct subregions.

As time progresses and the activity front advances outward, this confinement gradually weakens. Figure 2(b) shows that at later times, once the activity has spread over a larger fraction of the domain, the distinction between the flow inside and outside the initially active region becomes less pronounced. Vorticity structures extend more uniformly across the system, and the flow approaches the statistically homogeneous active turbulence state associated with the spatially averaged level of activity.

This gradual loss of confinement reflects the continuous reorganization of the flow in response to the evolving activity distribution. As regions of elevated activity are

advected and stretched, they generate local bursts of vorticity that seed turbulent motion in previously inactive regions. In this sense, the activity field acts as a moving, deformable source of turbulence whose spatial extent and intensity evolve dynamically in time.

The strong coupling between activity heterogeneity and flow structure is further highlighted in Fig. 2(c), which shows the magnitude of the activity gradient field,  $|\nabla\alpha(\mathbf{x}, t)|$ , at late times. The gradient field exhibits intermittent, worm-like structures with large amplitudes, reminiscent of scalar dissipation structures in turbulent flows. These regions of strong gradients tend to align with zones of intense vorticity and strain, indicating that sharp activity fronts not only mark transitions between dynamical regimes, but also actively participate in shaping the local flow. We refer the reader to Ref. [63] which shows the time evolution of these fields highlighting the transitions discussed above.

Overall, these results reinforce the interpretation of activity as an *active scalar*: Its spatial distribution governs where and how turbulent motion is generated, while the resulting flow feeds back to sharpen gradients, stretch fronts, and create complex filamentary structures. Even as the system evolves toward a homogeneous activity state at long times, the transient dynamics are dominated by this intricate co-evolution of activity and flow.

### C. Spectral signatures of heterogeneous activity and transient universality

We now turn to the spectral consequences of the evolving activity field and its impact on the structure of active turbulence. As established in Fig. 1 and Fig. 2, the advected activity field  $\alpha(\mathbf{x}, t)$  dynamically partitions the domain into regions that sustain qualitatively different dynamics. In particular, regions with  $\alpha < \alpha_c \approx -5$  support strongly chaotic and intermittent active turbulence, while regions with  $\alpha > \alpha_c$  remain weakly active and comparatively quiescent. The spatial extent of the strongly active regions therefore introduces a time-dependent and physically meaningful length scale into the problem, which we denote by  $R(t)$ .

Figure 3 shows how this evolving spatial structure is reflected in the kinetic energy spectra and related statistical measures for a system initialized with an extreme activity contrast,  $\alpha_{\text{in}} = -8$  and  $\alpha_{\text{out}} = 4$ , and with  $\text{Sc} = 1.8$ . This choice is made to clearly expose the mechanism underlying the coexistence of distinct spectral regimes and the eventual loss of universal behavior; qualitatively similar trends are also observed for less extreme values (e.g.  $\alpha_{\text{in}} = -6$  and  $\alpha_{\text{out}} = 0$ ), but the non-monotonic evolution of the crossover scale and the disappearance of the  $k^{-3/2}$  regime are most clearly resolved in this case.

Figure 3(a) displays the kinetic energy spectra  $E_k$  at four representative times. At early times, the spectrum exhibits two distinct scaling regimes. At larger wavenumbers, the spectrum follows the universal  $k^{-3/2}$  scaling previously identified in homogeneous systems with  $\alpha < \alpha_c$ , reflecting strongly active turbulent dynamics. At smaller wavenumbers, however, the spectrum crosses over to a non-universal scaling associated with weakly active regions. The coexistence of these regimes indicates that, during this transient phase, the flow simultaneously samples both strongly and weakly active environments.

The crossover between the two scaling regimes occurs at a time-dependent wavenumber  $k_R(t) \sim R^{-1}(t)$ , where  $R(t)$  is the instantaneous linear size of the region satisfying  $\alpha < \alpha_c$ . This crossover scale is not imposed externally, but emerges dynamically from the evolving activity field. Its real-space origin is made explicit in Fig. 3(b), which shows snapshots of the activity field  $\alpha(\mathbf{x}, t)$  at the same four times, with regions where  $\alpha < \alpha_c$  marked with a blue colormap. These blue regions directly define  $R(t)$  and coincide with the zones where intense vorticity and chaotic motion are sustained, as previously seen in Fig. 2.

At early times, the blue region in Fig. 3(b) forms a compact but growing patch. Length scales smaller than  $R(t)$  are therefore dominated by fluctuations arising within the strongly active environment and give rise to the universal  $k^{-3/2}$  scaling observed at large wavenumbers in Fig. 3(a). In contrast, length scales comparable to or larger than  $R(t)$  necessarily sample both strongly and weakly active regions, leading to a breakdown of universality and a crossover to non-universal scaling. As time

progresses, the snapshots in Fig. 3(b) show that the spatial extent of the region with  $\alpha < \alpha_c$  initially increases due to advection and stretching of the activity patch. Correspondingly,  $R(t)$  grows and the crossover wavenumber  $k_R(t)$  shifts to smaller values, allowing the universal  $k^{-3/2}$  scaling to extend to progressively larger scales in Fig. 3(a).

At later times, diffusion and mixing progressively smooth out activity gradients. The blue regions in Fig. 3(b) shrink and eventually become negligible, indicating that no extended region with  $\alpha < \alpha_c$  survives. This erosion of the strongly active core causes the crossover wavenumber  $k_R(t)$  to shift back toward larger values and ultimately eliminates the  $k^{-3/2}$  regime altogether, leaving a single non-universal spectral scaling once the activity field becomes sufficiently homogeneous. While Figs 3(a) and (b) are self-consistent and reflect the phenomenological argument developed above, finding a clear quantitative measurement of  $R(t)$  (and hence  $k_R(t)$ ), and their variation with the Schmidt number, is less trivial in such heterogeneous systems and left for future work.

The connection between the spatial evolution of the activity field and the spectral behavior is further reinforced in the inset of Fig. 3(c), which shows the probability density functions (PDFs) of the activity field  $\alpha$  at the same four times. At early times, the PDFs are close to bimodal, reflecting the sharp spatial segregation between the strongly active patch and the weakly active background seen in Fig. 3(b). As time evolves, the PDFs progressively flatten with vanishing contributions for  $\alpha \lesssim \alpha_c (= -5)$ , while still peaking at the right, indicating enhanced mixing and homogenization of the activity field. By the latest time, the disappearance of a tail below  $\alpha_c$  confirms that strongly active regions no longer persist, consistent with the absence of universal scaling in the energy spectra.

Additional insight into the fluctuations of the activity field is gained by monitoring the evolution of the  $\alpha$ -spectrum  $E_k^\alpha = \langle |\alpha_k|^2 \rangle$ , where  $\alpha_k$  are the Fourier modes of the activity field. The spectral evolution of the activity field is shown in Fig. 3(c) for the same four times as in Fig. 3(a) and (b). At early times, the activity spectrum exhibits an approximate  $k^{-2}$  scaling over an intermediate range of wavenumbers. This behavior originates from the presence of sharp, shock-like interfaces separating strongly and weakly active regions, as visible in the corresponding activity snapshots in Fig. 3(b). Such discontinuity-dominated structures naturally give rise to  $k^{-2}$  spectra [70].

At later times, advection and diffusion progressively smooth these sharp activity gradients, and the spectrum steepens toward a  $k^{-4}$  decay, consistent with an increasingly smooth activity field. Further, an intermediate  $k^{-1}$  regime is observed. While this scaling is reminiscent of the Batchelor regime for passively advected scalars [71], we emphasize that activity here is not passive and directly feeds back onto the flow; the resemblance is there-

fore purely qualitative at this stage and any equivalence between the two is left for future work.

This interpretation is further supported by the inset of Fig. 3(c), which shows the probability density functions (PDFs) of the activity field at the same times. At early times, the PDFs are near-bimodal, reflecting the coexistence of strongly active ( $\alpha < \alpha_c$ ) and weakly active regions. As time progresses, the distribution smoothens and the low- $\alpha$  tail progressively disappears. At late times, the PDFs show negligible probability for  $\alpha \lesssim \alpha_c \simeq -5$ , indicating the erosion of strongly active patches. Consistently, the universal  $k^{-3/2}$  scaling in the kinetic energy spectrum [Fig. 3(a)] vanishes at these times, confirming that the loss of strongly active regions directly eliminates the universal turbulent regime.

Taken together, Fig. 3 demonstrates that the emergence, evolution, and eventual disappearance of universal  $k^{-3/2}$  scaling in heterogeneous active turbulence can be traced directly to the spatiotemporal evolution of the activity field. The key control parameter is not the globally averaged activity (which remains constant), but the instantaneous size  $R(t)$  of regions satisfying  $\alpha < \alpha_c$ . Universality is therefore local in space and transient in time: It appears only on scales smaller than  $R(t)$  and persists only as long as strongly active patches survive. As advection, diffusion, and mixing reshape the activity field, the window of universal behavior shifts dynamically across scales and ultimately closes once the activity becomes homogeneous. Naturally, this window becomes shorter with a decreasing Sc number which accelerates activity homogenization.

## VII. CONCLUSIONS AND DISCUSSIONS

In this work, we have presented a combined review and theoretical study of turbulence-like states in dense active fluids, with particular emphasis on bacterial suspensions and related systems described by Toner–Tu–Swift–Hohenberg-type hydrodynamics. Building on earlier experimental and theoretical developments, we revisited the analogy between active turbulence and classical inertial turbulence, clarified its domain of validity, and highlighted the distinct nonequilibrium mechanisms that underlie chaotic flow generation in active matter.

A central message of this study is that active turbulence does not constitute a single universal state, but instead spans multiple dynamical regimes even simultaneously, controlled by activity, confinement, and nonlinear interactions. While homogeneous active systems can exhibit a transition to a strongly chaotic regime with universal spectral behavior and intermittency, real active systems are often spatially heterogeneous. Motivated by this observation, we focused on the role of spatially varying activity and introduced a minimal framework in which activity is treated as a dynamically evolving field advected by the flow it generates.

Our numerical results demonstrate that an advected

activity field gives rise to sharp activity fronts, transient confinement of turbulent motion, and complex interfacial morphologies. These fronts act as dynamical boundaries that partition the domain into regions with qualitatively distinct dynamics. As a consequence, energy spectra can exhibit coexisting scaling regimes associated with strongly and weakly active regions, with a crossover scale set by the instantaneous spatial extent of the strongly active patches. As activity is mixed and homogenized by advection and diffusion, this crossover shifts in time and the universal regime may ultimately disappear. Universality in active turbulence is therefore inherently local in space and transient in time in heterogeneous systems. The emergence of strongly heterogeneous and dynamically evolving flow structures in the presence of advected activity suggests additional physical consequences beyond spectral statistics. In classical inertial turbulence, coherent flow structures are known to play a central role in collision rates, coalescence, and transport processes [72, 73]. Our results raise the possibility that analogous structure-mediated interactions may arise in biological active flows, where activity heterogeneity could indirectly regulate encounters, mixing, and collective behavior.

An important direction for future work concerns the mathematical structure and higher-dimensional generalizations of the hydrodynamic equations underlying active turbulence. Recent analytical studies have begun to rigorously characterize the Toner–Tu and Toner–Tu–Swift–Hohenberg equations, addressing questions of well-posedness, global attractors, and bounds on solutions in two dimensions [58, 74, 75]. Such results provide a valuable theoretical foundation for the phenomenological and numerical observations reported here, particularly in regimes where strong activity and nonlinear advection lead to highly chaotic dynamics. Extending these mathematical analyses to settings with spatially heterogeneous and dynamically evolving activity fields remains an open challenge.

Equally important is the extension of active turbulence studies beyond quasi-two-dimensional geometries. While most experimental and theoretical work, including the present study, has focused on effectively two-dimensional systems, recent investigations have explored active turbulence in fully three-dimensional fluids [6, 76]. Understanding how activity heterogeneity, front dynamics, and transient universality manifest in three dimensions is a natural and necessary next step. Progress along these lines would help bridge minimal hydrodynamic models with more realistic biological and synthetic active systems and clarify the extent to which the concepts of confinement, crossover scales, and local universality identified here persist in higher dimensions.

In summary, treating activity as a dynamical, spatially structured field reveals new mechanisms by which turbulence-like states in active matter are organized, sustained, and ultimately destroyed. By explicitly accounting for the interplay between advection, diffusion, and

activity-dependent forcing, this work provides a framework for understanding active turbulence in more realistic, heterogeneous environments, and highlights the central role of activity fronts and interfaces in shaping non-equilibrium chaotic flows.

## ACKNOWLEDGMENTS

SM and SSR thank the Indo–French Centre for Applied Mathematics (IFCAM) for financial support. The simulations were performed on the ICTS clusters *Tetris* and *Contra*. SM acknowledges the IITK Initiation Grant project IITK/ME/2024316 and the Govt. of India grant ANRF/ECRG/2024/002467/ENS. SM would like to thank ICTS-TIFR for their hospitality and support. SS and SSR acknowledge support of the Department of Atomic Energy, Government of India, under project no. RTI4019.

- 
- [1] J. Toner, Y. Tu, and S. Ramaswamy, Hydrodynamics and phases of flocks, *Annals of Physics* **318**, 170 (2005), special Issue.
- [2] S. Ramaswamy, The mechanics and statistics of active matter, *Annual Review of Condensed Matter Physics* **1**, 323 (2010).
- [3] T. Vicsek and A. Zafeiris, Collective motion, *Physics Reports* **517**, 71 (2012), collective motion.
- [4] M. C. Marchetti, J. F. Joanny, S. Ramaswamy, T. B. Liverpool, J. Prost, M. Rao, and R. A. Simha, Hydrodynamics of soft active matter, *Rev. Mod. Phys.* **85**, 1143 (2013).
- [5] S. Ramaswamy, Active matter, *Journal of Statistical Mechanics: Theory and Experiment* **2017**, 054002 (2017).
- [6] R. Alert, J. Casademunt, and J.-F. Joanny, Active turbulence, *Annual Review of Condensed Matter Physics* **13**, 143 (2022).
- [7] X.-L. Wu and A. Libchaber, Particle diffusion in a quasi-two-dimensional bacterial bath, *Physical review letters* **84**, 3017 (2000).
- [8] T. Sanchez, D. T. N. Chen, S. J. DeCamp, M. Heymann, and Z. Dogic, Spontaneous motion in hierarchically assembled active matter, *Nature* **491**, 431 (2012).
- [9] J. R. Howse, R. A. L. Jones, A. J. Ryan, T. Gough, R. Vafabakhsh, and R. Golestanian, Self-motile colloidal particles: From directed propulsion to random walk, *Phys. Rev. Lett.* **99**, 048102 (2007).
- [10] V. Narayan, S. Ramaswamy, and N. Menon, Long-lived giant number fluctuations in a swarming granular nematic, *Science* **317**, 105 (2007).
- [11] T. Vicsek, A. Czirók, E. Ben-Jacob, I. Cohen, and O. Shochet, Novel type of phase transition in a system of self-driven particles, *Phys. Rev. Lett.* **75**, 1226 (1995).
- [12] A. Choudhary, D. Venkataraman, and S. Sankar Ray, Effect of inertia on model flocks in a turbulent environment, *Europhysics Letters* **112**, 24005 (2015).
- [13] A. Gupta, A. Roy, A. Saha, and S. S. Ray, Flocking of active particles in a turbulent flow, *Phys. Rev. Fluids* **5**, 052601 (2020).
- [14] H. P. Zhang, A. Be'er, E.-L. Florin, and H. L. Swinney, Collective motion and density fluctuations in bacterial colonies, *Proceedings of the National Academy of Sciences* **107**, 13626 (2010), <https://www.pnas.org/doi/pdf/10.1073/pnas.1001651107>.
- [15] F. Peruani, J. Starruß, V. Jakovljevic, L. Søgaard-Andersen, A. Deutsch, and M. Bär, Collective motion and nonequilibrium cluster formation in colonies of gliding bacteria, *Phys. Rev. Lett.* **108**, 098102 (2012).
- [16] G. Ariel, A. Rabani, S. Benisty, J. D. Partridge, R. M. Harshey, and A. Be'Er, Swarming bacteria migrate by lévy walk, *Nature communications* **6**, 8396 (2015).
- [17] J. Tailleur and M. E. Cates, Statistical mechanics of interacting run-and-tumble bacteria, *Phys. Rev. Lett.* **100**, 218103 (2008).
- [18] Y. Fily and M. C. Marchetti, Athermal phase separation of self-propelled particles with no alignment, *Phys. Rev. Lett.* **108**, 235702 (2012).
- [19] G. S. Redner, M. F. Hagan, and A. Baskaran, Structure and dynamics of a phase-separating active colloidal fluid, *Phys. Rev. Lett.* **110**, 055701 (2013).
- [20] R. Aditi Simha and S. Ramaswamy, Hydrodynamic fluctuations and instabilities in ordered suspensions of self-propelled particles, *Phys. Rev. Lett.* **89**, 058101 (2002).
- [21] R. Voituriez, J. F. Joanny, and J. Prost, Spontaneous flow transition in active polar gels, *Europhysics Letters* **70**, 404 (2005).
- [22] D. Marenduzzo, E. Orlandini, and J. M. Yeomans, Hydrodynamics and rheology of active liquid crystals: A numerical investigation, *Phys. Rev. Lett.* **98**, 118102 (2007).
- [23] P. Jain, N. Rana, S. Ramaswamy, and P. Perlekar, Inertia drives concentration-wave turbulence in swimmer suspensions, *Phys. Rev. Lett.* **133**, 158302 (2024).
- [24] H. H. Wensink, J. Dunkel, S. Heidenreich, K. Drescher, R. E. Goldstein, H. Löwen, and J. M. Yeomans, Mesoscale turbulence in living fluids, *Proceedings of the national academy of sciences* **109**, 14308 (2012).
- [25] J. Dunkel, S. Heidenreich, K. Drescher, H. H. Wensink, M. Bär, and R. E. Goldstein, Fluid dynamics of bacterial turbulence, *Physical review letters* **110**, 228102 (2013).
- [26] V. Bratanov, F. Jenko, and E. Frey, New class of turbulence in active fluids, *Proceedings of the National Academy of Sciences* **112**, 15048 (2015).
- [27] M. James, W. J. Bos, and M. Wilczek, Turbulence and turbulent pattern formation in a minimal model for active fluids, *Physical Review Fluids* **3**, 061101 (2018).
- [28] S. Mukherjee, R. K. Singh, M. James, and S. S. Ray, Anomalous diffusion and lévy walks distinguish active from inertial turbulence, *Physical Review Letters* **127**, 118001 (2021).
- [29] R. K. Singh, S. Mukherjee, and S. S. Ray, Lagrangian manifestation of anomalies in active turbulence, *Physical Review Fluids* **7**, 033101 (2022).

- [30] S. Mukherjee, R. K. Singh, M. James, and S. S. Ray, Intermittency, fluctuations and maximal chaos in an emergent universal state of active turbulence, *Nature Physics* **19**, 891 (2023).
- [31] K. V. Kiran, K. Kumar, A. Gupta, R. Pandit, and S. S. Ray, Onset of intermittency and multiscaling in active turbulence, *Phys. Rev. Lett.* **134**, 088302 (2025).
- [32] J. Toner and Y. Tu, Long-range order in a two-dimensional dynamical XY model: How birds fly together, *Phys. Rev. Lett.* **75**, 4326 (1995).
- [33] J. Toner and Y. Tu, Flocks, herds, and schools: A quantitative theory of flocking, *Phys. Rev. E* **58**, 4828 (1998).
- [34] J. Swift and P. C. Hohenberg, Hydrodynamic fluctuations at the convective instability, *Phys. Rev. A* **15**, 319 (1977).
- [35] M. C. Cross and P. C. Hohenberg, Pattern formation outside of equilibrium, *Rev. Mod. Phys.* **65**, 851 (1993).
- [36] S. Mukherjee, K. Kumar, and S. S. Ray, Turbulence-induced fluctuating interfaces in heterogeneously-active suspensions (2025), arXiv:2502.16443 [cond-mat.soft].
- [37] R. Thar and M. Köhl, Bacteria are not too small for spatial sensing of chemical gradients: an experimental evidence, *Proceedings of the National Academy of Sciences* **100**, 5748 (2003).
- [38] J. Arlt, V. A. Martinez, A. Dawson, T. Pilizota, and W. C. Poon, Painting with light-powered bacteria, *Nature communications* **9**, 768 (2018).
- [39] G. Frangipane, D. Dell'Arciprete, S. Petracchini, C. Maggi, F. Saglimbeni, S. Bianchi, G. Viznyiczai, M. L. Bernardini, and R. Di Leonardo, Dynamic density shaping of photokinetic *e. coli*, *Elife* **7**, e36608 (2018).
- [40] J. Arlt, V. A. Martinez, A. Dawson, T. Pilizota, and W. C. Poon, Dynamics-dependent density distribution in active suspensions, *Nature communications* **10**, 2321 (2019).
- [41] D. Nishiguchi, I. S. Aranson, A. Snezhko, and A. Sokolov, Engineering bacterial vortex lattice via direct laser lithography, *Nature communications* **9**, 4486 (2018).
- [42] H. Reinken, D. Nishiguchi, S. Heidenreich, A. Sokolov, M. Bär, S. H. Klapp, and I. S. Aranson, Organizing bacterial vortex lattices by periodic obstacle arrays, *Communications Physics* **3**, 76 (2020).
- [43] H. Reinken, S. Heidenreich, M. Bär, and S. H. Klapp, Ising-like critical behavior of vortex lattices in an active fluid, *Physical Review Letters* **128**, 048004 (2022).
- [44] J. Palacci, S. Sacanna, A. P. Steinberg, D. J. Pine, and P. M. Chaikin, Living crystals of light-activated colloidal surfers, *Science* **339**, 936 (2013).
- [45] M. Schuppler, F. C. Keber, M. Kröger, and A. R. Bausch, Boundaries steer the contraction of active gels, *Nature communications* **7**, 13120 (2016).
- [46] T. D. Ross, H. J. Lee, Z. Qu, R. A. Banks, R. Phillips, and M. Thomson, Controlling organization and forces in active matter through optically defined boundaries, *Nature* **572**, 224 (2019).
- [47] R. Zhang, S. A. Redford, P. V. Ruijgrok, N. Kumar, A. Mozaffari, S. Zemsky, A. R. Dinner, V. Vitelli, Z. Bryant, M. L. Gardel, *et al.*, Spatiotemporal control of liquid crystal structure and dynamics through activity patterning, *Nature materials* **20**, 875 (2021).
- [48] R. Zhang, A. Mozaffari, and J. J. de Pablo, Autonomous materials systems from active liquid crystals, *Nature Reviews Materials* **6**, 437 (2021).
- [49] S. Shankar, A. Souslov, M. J. Bowick, M. C. Marchetti, and V. Vitelli, Topological active matter, *Nature Reviews Physics* **4**, 380 (2022).
- [50] L. M. Lemma, M. Varghese, T. D. Ross, M. Thomson, A. Baskaran, and Z. Dogic, Spatio-temporal patterning of extensile active stresses in microtubule-based active fluids, *PNAS nexus* **2**, pgad130 (2023).
- [51] W. D. Hoff, M. A. van der Horst, C. B. Nudel, and K. J. Hellingwerf, Prokaryotic phototaxis, *Chemotaxis: Methods and Protocols*, 25 (2009).
- [52] A. Wilde and C. W. Mullineaux, Light-controlled motility in prokaryotes and the problem of directional light perception, *FEMS microbiology reviews* **41**, 900 (2017).
- [53] M. James and M. Wilczek, Vortex dynamics and lagrangian statistics in a model for active turbulence, *The European Physical Journal E* **41**, 1 (2018).
- [54] M. James, D. A. Suchla, J. Dunkel, and M. Wilczek, Emergence and melting of active vortex crystals, *Nature communications* **12**, 5630 (2021).
- [55] K. V. Kiran, A. Gupta, A. K. Verma, and R. Pandit, Irreversibility in bacterial turbulence: Insights from the mean-bacterial-velocity model, *Phys. Rev. Fluids* **8**, 023102 (2023).
- [56] P. Jain, N. Rana, R. Benzi, and P. Perlekar, Instabilities and turbulence in extensile swimmer suspensions, *Phys. Rev. Fluids* **10**, 114602 (2025).
- [57] K. Kashyap, K. V. Kiran, and A. Gupta, Emergence of local ordering and giant number fluctuations in active turbulence (2025), arXiv:2507.04890 [physics.flu-dyn].
- [58] R. Pandit and K. V. Kiran, Particles and fields in minimal hydrodynamic models for active turbulence, *Europhysics Letters* **150**, 13001 (2025).
- [59] J. Yang, P. E. Arratia, A. E. Patteson, and A. Gopinath, Quenching active swarms: effects of light exposure on collective motility in swarming *serratia marcescens*, *Journal of the Royal Society Interface* **16**, 20180960 (2019).
- [60] B. V. Hokmabad, A. Martínez-Calvo, S. G. L. Corte, and S. S. Datta, Spatial self-organization of confined bacterial suspensions, *Proceedings of the National Academy of Sciences* **122**, e2503983122 (2025).
- [61] A. Martínez-Calvo, C. Trenado-Yuste, H. Lee, J. Gore, N. S. Wingreen, and S. S. Datta, Interfacial morphodynamics of proliferating microbial communities, *Physical Review X* **15**, 011016 (2025).
- [62] See <https://youtu.be/X5eL8jaHwSU> for an animation illustrating the front morphologies of an active patch (confined initially inside a central disk) with varying Schmidt number. (2026).
- [63] See [https://youtu.be/pLi0L\\_4zKRw](https://youtu.be/pLi0L_4zKRw) for an animation showing the evolution of heterogeneous activity in bacterial turbulence while it feeds onto the flow. (2026).
- [64] S. Sahoo and S. S. Ray, Fluctuating interfaces in barotropic beta-plane turbulence (2025), arXiv:2507.23493 [physics.flu-dyn].
- [65] D. K. Bisset, J. C. Hunt, and M. M. Rogers, The turbulent/non-turbulent interface bounding a far wake, *Journal of Fluid Mechanics* **451**, 383 (2002).
- [66] J. Westerweel, C. Fukushima, J. M. Pedersen, and J. C. Hunt, Momentum and scalar transport at the turbulent/non-turbulent interface of a jet, *Journal of Fluid Mechanics* **631**, 199 (2009).
- [67] K. Chauhan, J. Philip, C. M. De Silva, N. Hutchins, and I. Marusic, The turbulent/non-turbulent interface and entrainment in a boundary layer, *Journal of Fluid Mechanics* **742**, 119 (2014).

- [68] G. Borrell and J. Jiménez, Properties of the turbulent/non-turbulent interface in boundary layers, *Journal of Fluid Mechanics* **801**, 554 (2016).
- [69] A. Mazzino and M. E. Rosti, Unraveling the secrets of turbulence in a fluid puff, *Physical Review Letters* **127**, 094501 (2021).
- [70] S. D. Murugan, U. Frisch, S. Nazarenko, N. Besse, and S. S. Ray, Suppressing thermalization and constructing weak solutions in truncated inviscid equations of hydrodynamics: Lessons from the burgers equation, *Phys. Rev. Res.* **2**, 033202 (2020).
- [71] G. K. Batchelor, Small-scale variation of convected quantities like temperature in turbulent fluid. part 1. general discussion and the case of small conductivity, *Journal of Fluid Mechanics* **5**, 113 (1959).
- [72] J. R. Picardo, L. Agasthya, R. Govindarajan, and S. S. Ray, Flow structures govern particle collisions in turbulence, *Phys. Rev. Fluids* **4**, 032601 (2019).
- [73] J. R. Picardo, R. Singh, S. S. Ray, and D. Vincenzi, Dynamics of a long chain in turbulent flows: impact of vortices, *Philosophical Transactions of the Royal Society A: Mathematical, Physical and Engineering Sciences* **378**, 20190405 (2020).
- [74] J. D. Gibbon, K. V. Kiran, N. B. Padhan, and R. Pandit, An analytical and computational study of the incompressible toner-tu equations, *Physica D: Nonlinear Phenomena* **444**, 133594 (2023).
- [75] D. W. Boutros, K. V. Kiran, J. D. Gibbon, and R. Pandit, The global attractor of the toner-tu-swift-hohenberg equations of active turbulence and its properties (2026), arXiv:2601.18233 [physics.flu-dyn].
- [76] P. Perlekar, Flocking and mesoscale turbulence in three-dimensional active fluids (2026), arXiv:2601.17674 [physics.flu-dyn].